



Solution-Processed Epitaxial Growth of MAPbI₃ Single-Crystal Films for Highly Stable Photodetectors

Yubing Xu¹, Xin Wang^{1*}, Jingda Zhao¹, Yuzhu Pan¹, Yuwei Li¹, Elias Emeka Elemike², Qing Li¹, Xiaobing Zhang¹, Jing Chen¹, Zhiwei Zhao¹, Javed Akram³, Byung Seong Bae⁴, Suhaidi Bin⁵ and Wei Lei^{1*}

¹ Joint International Research Laboratory of Information Display and Visualization, School of Electronic Science and Engineering, Southeast University, Nanjing, China, ² Department of Chemistry, Federal University of Petroleum Resources Effurun, Warri, Nigeria, ³ COMSATS University Islamabad (CUI), Islamabad, Pakistan, ⁴ Department of Electronics and Display Engineering, Hoseo University, Asan-si, South Korea, ⁵ Institute of Advanced Technology, Putra Malaysia University, Seri Kembangan, Malaysia

OPEN ACCESS

Edited by:

Fabian Ifeanyichukwu Ezema,
University of Nigeria, Nsukka, Nigeria

Reviewed by:

Hock Jin Quah,
University of Science Malaysia,
Malaysia
Martin Munz,
Helmholtz Association of German
Research Centers (HZ), Germany

*Correspondence:

Xin Wang
230159424@seu.edu.cn
Wei Lei
lw@seu.edu.cn

Specialty section:

This article was submitted to
Colloidal Materials and Interfaces,
a section of the journal
Frontiers in Materials

Received: 11 January 2021

Accepted: 22 March 2021

Published: 09 April 2021

Citation:

Xu Y, Wang X, Zhao J, Pan Y, Li Y, Elemike EE, Li Q, Zhang X, Chen J, Zhao Z, Akram J, Bae BS, Bin S and Lei W (2021) Solution-Processed Epitaxial Growth of MAPbI₃ Single-Crystal Films for Highly Stable Photodetectors. *Front. Mater.* 8:651957. doi: 10.3389/fmats.2021.651957

Recent years, organic-inorganic hybrid perovskites (OIHPs) have been widely used in applications, such as solar cells, lasers, light-emission diodes, and photodetectors due to their outstanding optoelectronic properties. Nowadays photodetectors based on perovskite films (PFs) suffer from surface and interface traps, which result from low crystalline quality of perovskite films and lattice mismatch between perovskite films and substrates. Herein, we fabricate MAPbI₃ (MA = CH₃NH₃) single-crystal films (SCFs) on MAPbBr₃ single crystal substrates in MAPbI₃ precursor solution during crystallization process via solution-processed epitaxy. Benefit from the good lattice matching, epitaxial MAPbI₃ SCFs with high crystallinity and smooth morphology are of comparable quality to MAPbI₃ PSCs and are of better quality than MAPbI₃ polycrystalline films. Here we report that epitaxial MAPbI₃ SCFs have a low trap density of 5.64 × 10¹¹ cm⁻³ and a long carrier lifetime of 11.86 μs. In this work, photodetector based on epitaxial MAPbI₃ single-crystal film (SCF) exhibits an excellent stability of a long-term stable response after 120 days, a fast response time of 2.21 μs, a high responsivity of 1.2 A W⁻¹ and a high detectivity of 3.07 × 10¹² jones.

Keywords: perovskite, epitaxial growth, photodetector, solution-processed, single-crystal film

INTRODUCTION

Organic-inorganic hybrid perovskites (OIHPs) have attracted worldwide numerous attention in recent years due to their remarkable properties in optoelectronic applications, such as solar cells, lasers, light-emission diodes and photodetectors (Shao et al., 2014; Tan et al., 2014; Wang et al., 2014, 2019a; Cho et al., 2015; Stranks and Snaith, 2015; Ling et al., 2016). As a new generation of promising semiconductor materials, solution-processable OIHPs are low-cost and have high absorption coefficient, tunable bandgap and long carrier lifetime and diffusion length (Xing et al., 2014; Fang et al., 2015; Wei et al., 2017). Up to now, not only devices based on perovskite single crystals (PSCs) have been widely used but also perovskite films (PFs)-based devices have shown great potential for high-performance photodetectors for visible light, near-infrared light

and high energy ray (Shao et al., 2014; Kim et al., 2017; Wang et al., 2018, 2020). For example, Kim et al. (2017) used MAPbI₃ films for large-area, low-dose X-ray imaging, Ji et al. (2018) reported OHIPs films-based photodetectors with high-performance and Hou et al. (2020) reported narrowband photodetectors based on mixed halide PFs. The critical factors of PFs-based devices are high crystallinity, smooth morphology of films and good lattice matching between layers to form high-quality epitaxial films on substrates, which result in low trap density, long carrier lifetimes, and long diffusion lengths (Shi et al., 2015; Ji et al., 2018; Tang et al., 2019; Chen et al., 2020). Although many epitaxy approaches, such as spin-coating method, vapor-phase epitaxy as well as van der Waals epitaxy have been used to grow PFs used for optoelectronic devices (Wang et al., 2015, 2021; Yang et al., 2015; Long et al., 2018; Kelso et al., 2019; Chen et al., 2020), it is also a challenge to overcome the lattice mismatching between epitaxial PFs and substrates and to obtain high-crystallinity PFs with smooth morphology and good stability. Furthermore, the high trap density, short carrier lifetimes and short diffusion length of epitaxial PFs have restricted the development of photodetectors based on PFs (Wang et al., 2014; Chen et al., 2015; Tong et al., 2017; Yang et al., 2017; Abdi-Jalebi et al., 2018).

Methylammonium lead halide perovskites (MAPbX₃, where X = Cl, Br, I) have been the most widely studied OIHPs (Wei et al., 2017; Jiang et al., 2019) and the lattice parameters of MAPbI₃ and MAPbBr₃ are calculated as 6.23 and 5.93 Å, respectively. The lattice mismatching rate is calculated to be only 4.81% at room temperature so that MAPbI₃ single-crystal films (SCFs) are able to be epitaxially grown on MAPbBr₃ single crystal substrate (Wang et al., 2020; Xu et al., 2020). Here in this work, Different from reported solution-processed epitaxy, such as spin-coating method, our work directly put MAPbBr₃ substrates into MAPbI₃ precursor solution. Benefit from good lattice matching, MAPbI₃ layers can directly grow on the surface of MAPbBr₃ substrates in MAPbI₃ precursor solution at optimal growth temperature during crystallization process. This method in our work can easily get high-quality epitaxial layers with high crystallinity, good morphology and thickness of micro level for stable photodetectors. The epitaxial MAPbI₃ SCFs are of comparable quality to MAPbI₃ PSCs and are of better quality than MAPbI₃ polycrystalline films. Furthermore, epitaxial MAPbI₃ SCFs with dense structure have much better stability than polycrystalline films. X-ray diffraction (XRD) is used to compare the crystallinity of epitaxial MAPbI₃ SCFs and scanning electron microscopy (SEM) is used to characterize the surface morphology and the thickness of epitaxial MAPbI₃ SCFs. Additionally, this work fabricate a high performance stable photodetector based on high-quality epitaxial MAPbI₃ SCFs on MAPbBr₃ single crystal substrate as well as a photodetector based on MAPbI₃ PSCs for comparison. Moreover, the trap density is characterized by space-charge-limited-current (SCLC) and the stability is exhibited by long-term dark currents and photocurrents. The high-crystallinity film has low trap density of $5.64 \times 10^{11} \text{ cm}^{-3}$ and long carrier lifetime of 11.86 μs. Briefly, this photodetector has outstanding optoelectronic performance

with a good stability, a fast response speed of 2.21 μs, a responsivity of 1.2 A W⁻¹ and a high detectivity of 3.07×10^{12} Jones.

MATERIALS AND METHODS

Preparation of CH₃NH₃I Powder and CH₃NH₃Br Powder

To get CH₃NH₃I powder, Hydroiodic Acid (40 wt% in water, Macklin) reacted with Methylamine (30–33 wt% in ethanol, Macklin) in a 50 ml bottle at 0°C for 2 h with stirring. After fully reaction, the mixed solution was heated to 100°C on a hot plate with magnetic stirring then the precipitate of CH₃NH₃I gradually appeared. The precipitate of CH₃NH₃I was washed in ether solution twice and was re-dissolved in absolute ethanol. The CH₃NH₃I powder was collected after dried at 75°C in a vacuum dryer (China) for 12 h. To get MAPbBr₃ powder, Hydrobromic Acid (55 wt% in water, Macklin) was mixed with Methylamine (30–33 wt% in ethanol, Macklin) and other steps are same as the synthesis of CH₃NH₃I powder.

Preparation of Precursor Solution

To get MAPbI₃ precursor solution, as-prepared CH₃NH₃I and Lead iodide (PbI₂, 99%, Sigma Aldrich) with a ratio of 1:1 were dissolved in anhydrous γ-butyrolactone (GBL, 99%, Aladdin). The final concentrations were 0.1 M Lead iodide and 0.1 M CH₃NH₃I mixed in 100 ml GBL solution. And MAPbBr₃ precursor solution was a N, N-Dimethylformamide (DMF, 99.5%, SCR) solution which dissolves as-prepared CH₃NH₃Br and lead bromine (PbBr₂, 98%, Sigma Aldrich) with a ratio of 1:1.

Device Fabrication

To grow high-quality MAPbBr₃ PSCs as substrate, the MAPbBr₃ precursor solution was heated in crystallizing dish in air from 55 to 80°C at a rate of 0.3°C h⁻¹. Then the MAPbBr₃ PSCs was put into MAPbI₃ precursor solution to grow epitaxial MAPbI₃ SCFs at 110°C. The absolute dichloromethane solution was used to wash off the remains of the precursor solution from the crystal surface. The programmable heating control system was realized on IKA-RET control-visc. The final device was cut by diamond wire (Φ0.35 mm) and polished by Glycerin and diamond powder (Φ0.5 μm) mixed solution. The cutting and polishing system (STX-202A, UNIPOL-802) was pursued from KEJING company (Shenyang, China). And the toluene solution was used to wash the mixed solution remaining on the surface of single crystal. The gold electrodes were deposited on the surface of MAPbI₃ single-crystal film by a metal shadow mask with 500 μm channel by thermal evaporation in vacuum.

Characterization

Scanning electron microscopy (SEM) images were taken with a Quanta 200 FEI (United States). Atomic force microscope (AFM) was obtained by Mulyimode-8-AM. X-ray diffraction (XRD) patterns were obtained by X'TRA (Switzerland). Photoluminescence (PL) spectra was measured by UV-vis spectroscopy (Lab Tech Bluestar, United States).

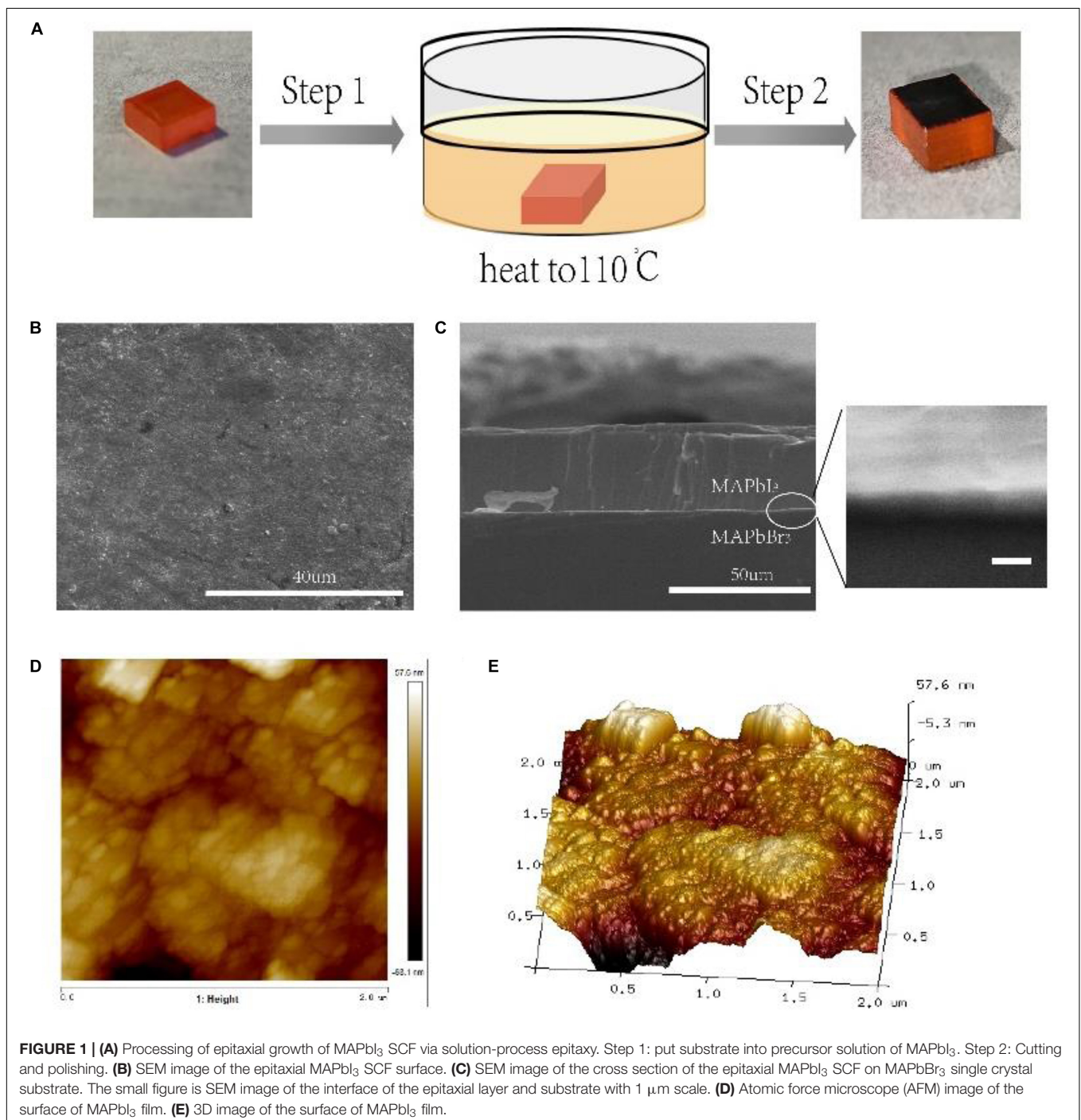
Device Performance Measurements

All measurements were performed on the probe station. Keithley 2410 was used as the voltage source to measure current-voltage curve (I-V) with 0.6 V/s voltage sweep rate. A 355 nm pulsed Nd:YAG laser with 6 ns pulse width at 20 Hz was used as the illumination source and response time was measured using an Agilent oscilloscope (DSO-X4054A) of KEYSIGHT. The 670 nm light source was obtained from L10762 of Hamamatsu. Agilent 81110A was used to power the light-emitting diode (LED). The

working voltage and current of XRD copper target ray tube is 40 KeV and 40 mA, respectively. And the emission laser of 450 nm is obtained from NBET-LASER.

RESULTS AND DISCUSSION

As illustrated in **Figure 1A**, a solution-processed epitaxy is employed to fabricate MAPbI₃ SCF on MAPbBr₃ single

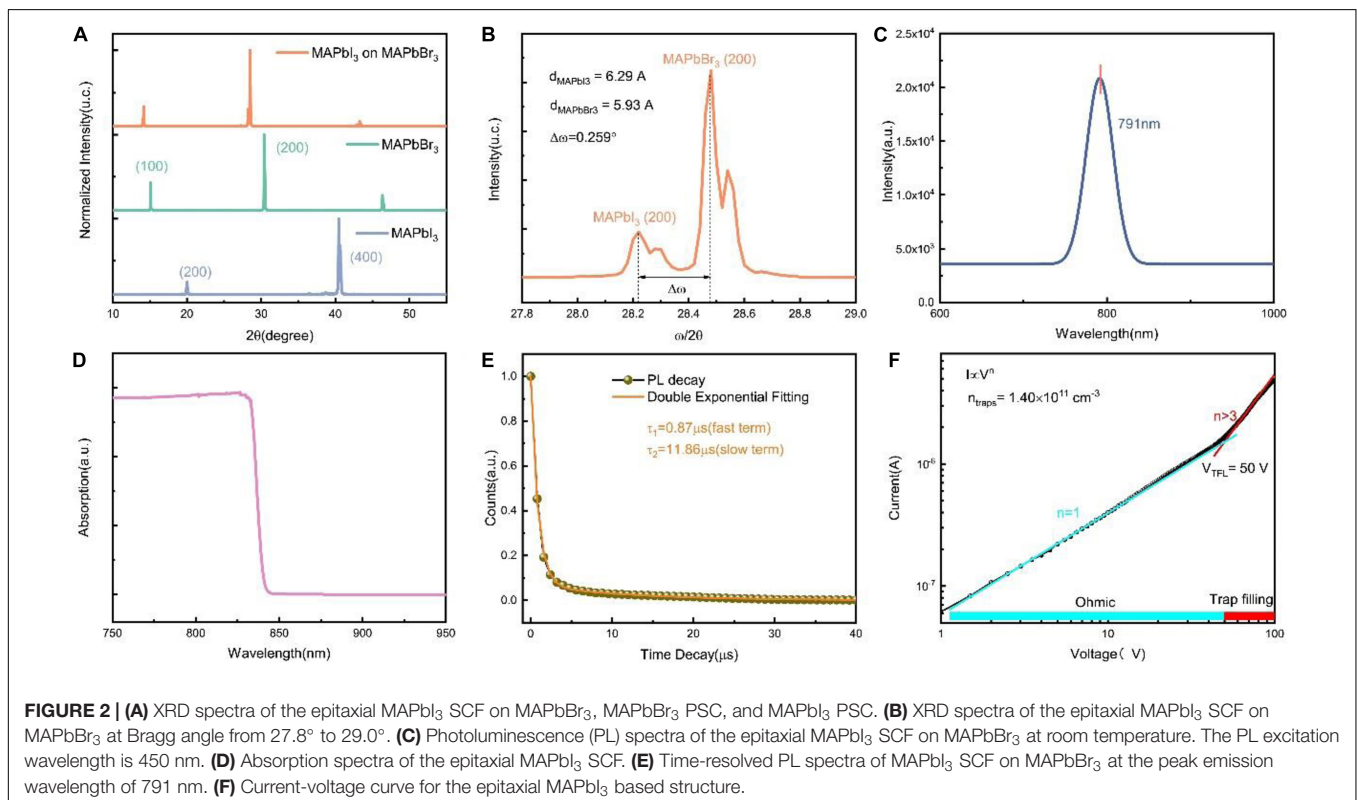


crystal substrate. Firstly, a high-quality MAPbBr₃ single crystal is put into the precursor solution of MAPbI₃ heated to 110°C at which the MAPbI₃ SCFs can be densely and rapidly grown on the whole surface of the substrate. Then, after cutting and polishing, a MAPbI₃ SCF is deposited on MAPbBr₃ (200) single crystal substrate. SEM images of the epitaxial MAPbI₃ SCF surface and the cross section of the epitaxial MAPbI₃ SCF on MAPbBr₃ demonstrate the morphology and thicknesses of epitaxial MAPbI₃ SCFs. As shown in **Figure 1B**, epitaxial MAPbI₃ SCF with smooth surface are grown densely on the MAPbBr₃ (200) single crystal substrate. Moreover, the thickness of epitaxial films is about 37.1 μm which are two orders of magnitude thicker than films deposited by spin-coating method (Wang et al., 2014; Fei et al., 2017; Ji et al., 2018), as clearly shown in **Figure 1C**. And the small picture in **Figure 1C** shows the interface of the epitaxial layer and substrate. Epitaxial MAPbI₃ SCF with smooth morphology and controllable thickness can be directly grown on MAPbBr₃ single crystal substrate due to good lattice matching (Li et al., 2020; Pan et al., 2020; Xu et al., 2020). As shown in **Figures 1D,E**, Atomic force microscope (AFM, Mulyimode-8-AM) was performed to further characterize the surface of MAPbI₃ film and the roughness is approximately 14.9 nm.

XRD and PL characterization are performed to determine the quality and crystallinity of the epitaxial MAPbI₃ SCFs. For comparison, the XRD spectra of the epitaxial MAPbI₃ on MAPbBr₃ (orange line), MAPbBr₃ PSC (green line) and MAPbI₃ PSC (blue line) are shown, respectively, in **Figure 2A**.

Different from MAPbI₃ single crystal of hexagonal structure, the epitaxial MAPbI₃ film changes to cubic structure because of the cubic MAPbBr₃ substrate (Wang et al., 2019b). Additionally, **Figure 2B** shows a clear MAPbI₃ (200) peak at a Bragg angle of $2\theta = 28.22^\circ$ and a MAPbBr₃ (200) peak at $2\theta = 28.47^\circ$. Furthermore, MAPbI₃ (200) peak with a full width at half-maximum (FWHM) of 0.0925 in **Figure 2B**, which is comparable to MAPbI₃ single crystal (200) peak with a FWHM of 0.1121, indicates the high crystallinity of epitaxial MAPbI₃ SCFs (Liu et al., 1991, 2016). **Figure 2C** demonstrates the steady-state PL spectra at room temperature with a strong emission peak at 791 nm under the 450 nm excitation with a FWHM of 32.3 nm, which is smaller than 60 nm of MAPbI₃ single crystal and 55 nm of MAPbI₃ polycrystalline film (Han et al., 2018), confirming the high quality of epitaxial film.

Moreover, **Figure 2D** illustrates that the absorption onset of epitaxial MAPbI₃ SCF is 840 nm, which are comparable to the 850 nm absorption onset of MAPbI₃ single crystal (Dong et al., 2015). And the redshift is obvious compared to the 780 nm absorption onset of polycrystalline MAPbI₃ film (Zhang et al., 2016). As shown in **Figure 2E**, double exponential fitting is performed to evaluate the carrier lifetime (τ) of epitaxial MAPbI₃ SCF. The short lifetime of $0.874 \pm 0.002 \mu\text{s}$ indicates surface recombination while long lifetime of $11.86 \pm 0.14 \mu\text{s}$ suggests bulk recombination (Shi et al., 2015). The carrier lifetime of epitaxial MAPbI₃ SCF is much longer than the carrier lifetime of polycrystalline film of nanosecond scale (Tong et al., 2017). In addition, space-charge-limited current (SCLC)



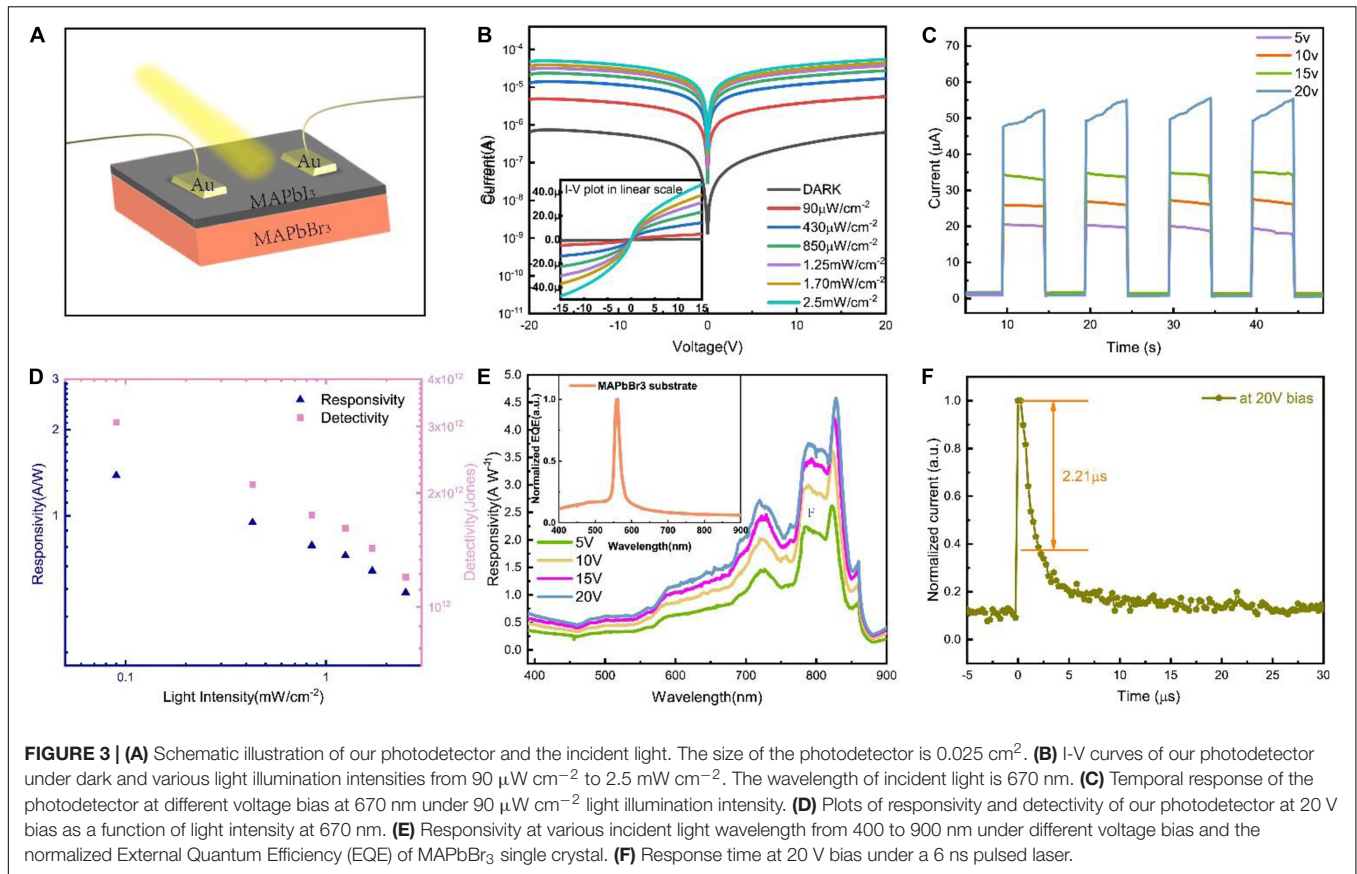


FIGURE 3 | (A) Schematic illustration of our photodetector and the incident light. The size of the photodetector is 0.025 cm². **(B)** I-V curves of our photodetector under dark and various light illumination intensities from 90 μW cm⁻² to 2.5 mW cm⁻². The wavelength of incident light is 670 nm. **(C)** Temporal response of the photodetector at different voltage bias at 670 nm under 90 μW cm⁻² light illumination intensity. **(D)** Plots of responsivity and detectivity of our photodetector at 20 V bias as a function of light intensity at 670 nm. **(E)** Responsivity at various incident light wavelength from 400 to 900 nm under different voltage bias and the normalized External Quantum Efficiency (EQE) of MAPbBr₃ single crystal. **(F)** Response time at 20 V bias under a 6 ns pulsed laser.

technique is used to estimate the trap density of epitaxial MAPbI₃ SCF (Rose, 1955). The formula is $n_{traps} = \frac{2\epsilon V_{TFL}}{qL^2}$, where ϵ is relative dielectric constant, V_{TFL} is the trap-filled limit voltage, q is the electronic charge. As to the horizontal device architecture in this work, L is the channel length between two gold electrodes, which were deposited on the surface of MAPbI₃ films by a shadow mask. As shown in Figure 2F, there is a linear current-voltage curve ($n = 1$) obeying Ohm's law since the injected charge carriers at low applied voltage is too weak to completely fill trap center. As the applied voltage gradually increases, the injected carrier concentration is greater than the thermally excited carrier concentration and the conduction law changes from the ohmic mode to the SCLC mode. When the applied voltage further increases, all injected charge carriers are used to fill deep traps and all traps will be filled at V_{TFL} (Quah and Cheong, 2013a,b). Figure 2F exhibits the current-voltage curve for the epitaxial MAPbI₃ based structure. The L is 500 μm with 1% error and V_{TFL} is 50 V so that the low trap density is calculated as $5.64(\pm 0.12) \times 10^{11}$ cm⁻³, which is much lower than polycrystalline films (Dong et al., 2015; Li et al., 2018). The high quality and crystallinity of epitaxial MAPbI₃ SCF benefit the wider absorption range, longer carrier lifetime and lower trap density than polycrystalline films.

To further validate the quality of the epitaxial MAPbI₃ SCF, a horizontal architecture photodetector with two golden electrodes

deposited on the surface of epitaxial MAPbI₃ SCF is fabricated as shown in Figure 3A. A light-emitting diode at 670 nm is used as light source for characterization of optoelectronic performance. Figures 3B,C plot the typical I-V curve under various light illumination intensities and the temporal response at different voltage bias of our photodetector, respectively. The dark current is very low of 7.1 nA at 0.2 V, which benefits the high photocurrent to dark current ratio (I_{ON}/I_{OFF}) of 331.7 with 2.5 mW cm⁻² light illumination. Additionally, responsivity ($R = \frac{J_{light} - J_{dark}}{P_{light}}$) and detectivity ($D = \frac{J_{light}}{P_{light} \sqrt{2qJ_{dark}}}$) are calculated to evaluate the performance of this photodetector (Gong et al., 2009; Zhang et al., 2018). As shown in Figure 3D, R is as high as 1.38 A W⁻¹ and the maximum D is 3.07×10^{12} jones at 20 V bias with 90 μW cm⁻² illumination at 670 nm, which are higher than polycrystalline films-based devices, reflecting the efficiency and ability of this photodetector responds to weak optical signal (Jiao et al., 2017; Wang et al., 2019c). Additionally, responsivities as a function of wavelength from 400 to 900 nm are illustrated in Figure 3E. And the normalized EQE of MAPbBr₃ single crystal in Figure 3E indicates that photodetectors based on epitaxial films can widen the absorption range of substrate. As shown in Figure 3F, a 6 ns pulsed laser is used to measure the response speed and it takes only 2.21 μs for current decay to 63% at 20 V bias, which is much faster than devices based on polycrystalline films, owing to the high quality of epitaxial MAPbI₃ SCF (Horvath et al., 2014; Mi et al., 2017; Wu et al., 2020).

To further indicate the high quality of epitaxial MAPbI₃ SCF, variable temperature crystallization (VTC) method (Wang et al., 2017) is employed for synthesis of MAPbI₃ PSC and a photodetector based on MAPbI₃ PSC is fabricated and tested under same test environment for comparison in this work. **Figures 4A,B** illustrate the dark current and the photocurrent with 90 μW cm⁻² illumination at 670 nm of epitaxial film-based device and PSC-based photodetector. Epitaxial film-based device has lower dark currents at voltages from 0.2 to 10.4 V bias and higher photocurrents than PSC-based photodetector. As shown in **Figure 4C**, the I_{ON}/I_{OFF} ratios of epitaxial film-based device are about 10 times higher than those of PSC-based photodetector. **Figure 4D** shows the dark current densities

at 20 V bias after various days, which of 25.3 μA cm⁻² on day 0 and of 33.11 μA cm⁻² on day 120. In addition, **Figure 4E** shows the long-term stable response of our device on day 120 at 20 V bias. The increasing rate formula is Rate = $\frac{(J_m - J_n)}{J_n} \times 100\%$, where J_m and J_n are the dark current densities on day m and day n. The calculated rate of change in dark current density is about 0.255% per day. The good morphology and crystallinity of epitaxial films benefit better stability than polycrystalline films (Salim et al., 2015; Taylor et al., 2020). The comparison of photoelectric performance between different MAPbI₃-based devices is shown in **Table 1**. The excellent performance actually validates the high-quality of the epitaxial MAPbI₃ SCFs.

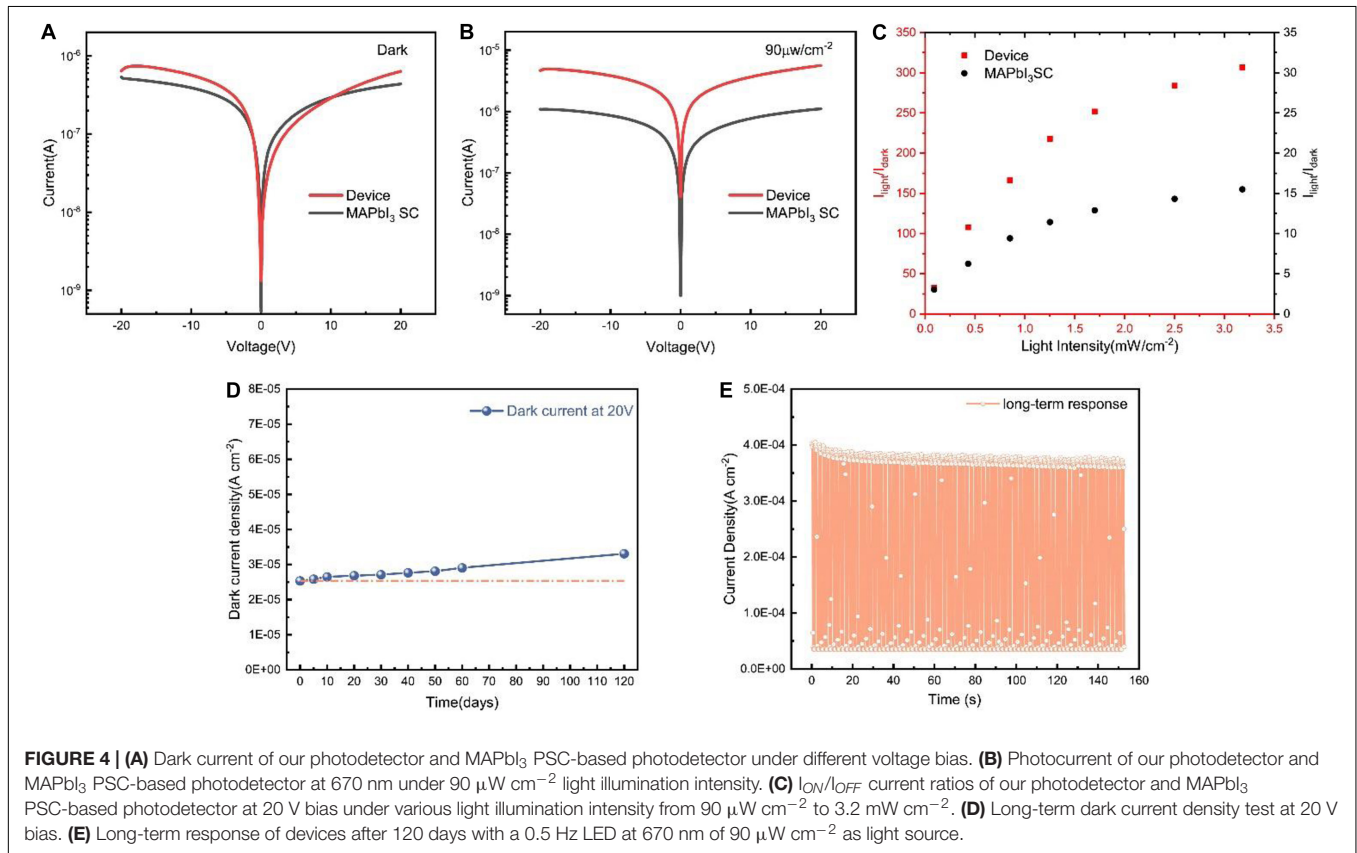


FIGURE 4 | (A) Dark current of our photodetector and MAPbI₃ PSC-based photodetector under different voltage bias. **(B)** Photocurrent of our photodetector and MAPbI₃ PSC-based photodetector at 670 nm under 90 μW cm⁻² light illumination intensity. **(C)** I_{ON}/I_{OFF} current ratios of our photodetector and MAPbI₃ PSC-based photodetector at 20 V bias under various light illumination intensity from 90 μW cm⁻² to 3.2 mW cm⁻². **(D)** Long-term dark current density test at 20 V bias. **(E)** Long-term response of devices after 120 days with a 0.5 Hz LED at 670 nm of 90 μW cm⁻² as light source.

TABLE 1 | Device performance comparison between MAPbI₃-based photodetectors.

Material (structure)	Detectivity (Jones)	Responsivity (A W ⁻¹)	I _{ON} /I _{OFF} Ratio	References
MAPbI ₃ single-crystal film	3.07 × 10 ¹²	1.2	10 ²	This work
MAPbI ₃ single crystal (lateral)	10 ¹⁰ –10 ¹²	0.15	10 ¹	Sun et al., 2017
MAPbI ₃ /TiO ₂ film	2.5 × 10 ¹⁰	2.4 mA W ⁻¹	10 ¹	Jiao et al., 2017
MAPbI ₃ film	1.22 × 10 ¹³	0.418	–	Zhang et al., 2018
MAPbI ₃ /PDPP3T films	1.5 × 10 ¹⁰	0.053	–	Yakunin et al., 2016
MAPbI ₃ network PD arrays	1.02 × 10 ¹²	0.12	–	Li et al., 2015
MAPbI ₃ film (lateral-MSM)	1.3 × 10 ¹¹	0.11	–	Wang et al., 2016
MAPbI ₃ nanoplates	–	60 mA W ⁻¹	10 ²	Qin et al., 2016
MAPbI ₃ nanowires	2.5 × 10 ¹²	1.32	–	Tang et al., 2016
ZnO/MAPbI ₃ nanowires (lateral)	1.74 × 10 ⁹	4	–	Qiao et al., 2016

CONCLUSION

In summary, this work demonstrates the epitaxial growth of high-quality MAPbI₃ single-crystal film on MAPbBr₃ substrate with good lattice matching. XRD, AFM, and SEM characterizations are performed to confirm the high crystalline and smooth morphology, which result in the low trap density of $5.64 \times 10^{11} \text{ cm}^{-3}$ and long carrier lifetime of 11.86 μs . Additionally, we fabricate a high-performance photodetector based on epitaxial MAPbI₃ SCF with responsivity of 1.2 A W^{-1} , detectivity of 3.07×10^{12} jones, response time of 2.21 μs and excellent stability for 120 days. Therefore, this epitaxial growth method provides a new path for high-stability perovskite film-based devices.

DATA AVAILABILITY STATEMENT

The raw data supporting the conclusions of this article will be made available by the authors, without undue reservation, to any qualified researcher.

REFERENCES

- Abdi-Jalebi, M., Pazoki, M., Philippe, B., Dar, M. I., Alsari, M., Sadhanala, A., et al. (2018). Dedoping of Lead Halide Perovskites Incorporating Monovalent Cations. *ACS Nano* 12, 7301–7311. doi: 10.1021/acsnano.8b03586
- Chen, Y., Lei, Y., Li, Y., Yu, Y., Cai, J., Chiu, M. H., et al. (2020). Strain engineering and epitaxial stabilization of halide perovskites. *Nature* 577, 209–215.
- Chen, Y., Peng, J., Su, D., Chen, X., and Liang, Z. (2015). Efficient and balanced charge transport revealed in planar perovskite solar cells. *ACS Appl. Mater. Interfaces* 7, 4471–4475. doi: 10.1021/acsami.5b00077
- Cho, H. C., Jeong, S. H., Park, M. H., Kim, Y. H., Wolf, C., Lee, C. L., et al. (2015). Overcoming the electroluminescence efficiency limitations of perovskite light-emitting diodes. *Science* 350, 1222–1225. doi: 10.1126/science.aad1818
- Dong, Q., Fang, Y., Shao, Y., Mulligan, P., Qiu, J., Cao, L., et al. (2015). Electron-hole diffusion lengths > 175 μm in solution-grown CH₃NH₃PbI₃ single crystals. *Science* 347, 967–970.
- Fang, Y., Dong, Q., Shao, Y., Yuan, Y., and Huang, J. (2015). Highly narrowband perovskite single-crystal photodetectors enabled by surface-charge recombination. *Nat. Photonics* 9, 679–686. doi: 10.1038/nphoton.2015.156
- Fei, C., Li, B., Zhang, R., Fu, H., Tian, J., and Cao, G. (2017). Highly efficient and stable perovskite solar cells based on monolithically grained CH₃NH₃PbI₃ film. *Adv. Energy Mater.* 7:1602017. doi: 10.1002/aenm.201602017
- Gong, X., Tong, M., Xia, Y., Cai, W., Moon, J. S., Cao, Y., et al. (2009). High-detectivity polymer photodetectors with spectral response from 300 nm to 1450 nm. *Science* 325, 1665–1667.
- Han, C., Wei, Z., Wang, K., Yu, H., Deng, L., Zhu, X., et al. (2018). Effect of surface recombination in high performance white-light CH₃NH₃PbI₃ single crystal photodetectors. *Opt. Express* 26, 26307–26316. doi: 10.1364/oe.26.026307
- Horvath, E., Spina, M., Szekrenyes, Z., Kamaras, K., Gaal, R., Gachet, D., et al. (2014). Nanowires of methylammonium lead iodide (CH₃NH₃PbI₃) prepared by low temperature solution-mediated crystallization. *Nano Lett.* 14, 6761–6766. doi: 10.1021/nl5020684
- Hou, Y., Wu, C., Huang, X., Yang, D., Ye, T., Yoon, J., et al. (2020). Self-powered Red/UV narrowband photodetector by unbalanced charge carrier transport strategy. *Adv. Funct. Mater.* 31:2007016. doi: 10.1002/adfm.202007016
- Ji, L., Hsu, H. Y., Lee, J. C., Bard, A. J., and Yu, E. T. (2018). High-performance photodetectors based on solution-processed epitaxial grown hybrid halide perovskites. *Nano Lett.* 18, 994–1000.
- Jiang, S., Wang, X., Wu, Y., Li, Y., Zhang, Q., Li, G., et al. (2019). Balance lead in solution-processed CH₃NH₃PbBr_xCl_(3-x) single crystals for high performance X-ray detection. *Mater. Lett.* 236, 26–29. doi: 10.1016/j.matlet.2018.10.055

AUTHOR CONTRIBUTIONS

YX, JZ, and YL grew the perovskite single crystals. YX and JZ did the epitaxial experiments. YX, YP, and JZ did the measurements. XW and YX analyzed these results. YX wrote the manuscript. All authors made comments on this manuscript.

FUNDING

This work was financially supported by the National Key Research and Development Program of China (2018YFE0125500, 2016YFB0401600), the Program 111_2.0 in China (BP0719013), the National Natural Science Foundation Project of China (61775034, 51879042, 61674029, 12005038), the Research Fund for International Young Scientists (62050410350), the International Cooperative Research Project of Jiangsu Province (BZ2018056), and the Leading Technology of Jiangsu Basic Research Plan (BK20192003).

- Jiao, S., Fu, X., Lian, G., Jing, L., Xu, Z., Wang, Q., et al. (2017). Ultrathin TiO₂nanosheets synthesized using a high pressure solvothermal method and the enhanced photoresponse performance of CH₃NH₃PbI₃-TiO₂composite films. *RSC Adv.* 7, 20845–20850. doi: 10.1039/c7ra01073g
- Kelso, M. V., Mahenderkar, N. K., Chen, Q., Tubbesing, J. Z., and Switzer, J. A. (2019). Spin coating epitaxial films. *Science* 364, 166–169.
- Kim, Y. C., Kim, K. H., Son, D. Y., Jeong, D. N., Seo, J. Y., Choi, Y. S., et al. (2017). Printable organometallic perovskite enables large-area, low-dose X-ray imaging. *Nature* 550, 87–91. doi: 10.1038/nature24032
- Li, F., Ma, C., Wang, H., Hu, W., Yu, W., Sheikh, A. D., et al. (2015). Ambipolar solution-processed hybrid perovskite phototransistors. *Nat. Commun.* 6:8238.
- Li, Y., Li, Y., Shi, J., Zhang, H., Wu, J., Li, D., et al. (2018). High quality perovskite crystals for efficient film photodetectors induced by hydrolytic insulating oxide substrates. *Adv. Funct. Mater.* 28:1705220. doi: 10.1002/adfm.201705220
- Li, Y.-W., Wang, X., Li, G.-W., Wu, Y., Pan, Y.-Z., Xu, Y.-B., et al. (2020). Fast liquid phase epitaxial growth for perovskite single crystals*. *Chin. Phys. Lett.* 37:018101. doi: 10.1088/0256-307x/37/1/018101
- Ling, Y., Yuan, Z., Tian, Y., Wang, X., Wang, J. C., Xin, Y., et al. (2016). Bright light-emitting diodes based on organometal halide perovskite nanoplatelets. *Adv. Mater.* 28, 305–311. doi: 10.1002/adma.201503954
- Liu, S., Lu, Y.-J., Kappes, M. M., and Ibers, J. A. (1991). The structure of the C60 molecule: x-ray crystal structure determination of a twin at 110 K. *Science* 254, 408–410. doi: 10.1126/science.254.5030.408
- Liu, Y., Zhang, Y., Yang, Z., Yang, D., Ren, X., Pang, L., et al. (2016). Thinness- and shape-controlled growth for ultrathin single-crystalline perovskite wafers for mass production of superior photoelectronic devices. *Adv. Mater.* 28, 9204–9209. doi: 10.1002/adma.201601995
- Long, G., Jiang, C., Sabatini, R., Yang, Z., Wei, M., Quan, L. N., et al. (2018). Spin control in reduced-dimensional chiral perovskites. *Nat. Photonics* 12, 528–533.
- Mi, B., Li, H., Song, Z., Zhao, G., Tong, G., and Jiang, Y. (2017). Hybrid perovskite photoconductivity visible region detector with high speed and stability. *Nano* 12:1750150. doi: 10.1142/s1793292017501508
- Pan, Y., Wang, X., Xu, Y., Li, Y., Elemike, E. E., Shuja, A., et al. (2020). Enhanced performance of perovskite single-crystal photodiodes by epitaxial hole blocking layer. *Front. Chem.* 8:791. doi: 10.3389/fchem.2020.00791
- Qiao, K., Deng, H., Yang, X., Dong, D., Li, M., Hu, L., et al. (2016). Spectra-selective PbS quantum dot infrared photodetectors. *Nanoscale* 8, 7137–7143. doi: 10.1039/c5nr09069e
- Qin, X., Yao, Y., Dong, H., Zhen, Y., Jiang, L., and Hu, W. (2016). Perovskite Photodetectors based on CH₃NH₃PbI₃ single crystals. *Chem. Asian J.* 11, 2675–2679.

- Quah, H. J., and Cheong, K. Y. (2013a). Current conduction mechanisms of RF-Magnetron sputtered Y2O3 gate oxide on gallium nitride. *Curr. Appl. Phys.* 13, 1433–1439. doi: 10.1016/j.cap.2013.04.028
- Quah, H. J., and Cheong, K. Y. (2013b). Surface passivation of gallium nitride by ultrathin RF-magnetron sputtered Al2O3 gate. *ACS Appl. Mater. Interfaces* 5, 6860–6863. doi: 10.1021/am402333t
- Rose, A. (1955). Space-charge-limited currents in solids. *Phys. Rev.* 97:1538. doi: 10.1103/physrev.97.1538
- Salim, T., Sun, S., Abe, Y., Krishna, A., Grimsdale, A. C., and Lam, Y. M. (2015). Perovskite-based solar cells: impact of morphology and device architecture on device performance. *J. Mater. Chem. A* 3, 8943–8969. doi: 10.1039/c4ta05226a
- Shao, Y., Xiao, Z., Bi, C., Yuan, Y., and Huang, J. (2014). Origin and elimination of photocurrent hysteresis by fullerene passivation in CH3NH3PbI3 planar heterojunction solar cells. *Nat. Commun.* 5:5784.
- Shi, D., Adinolfi, V., Comin, R., Yuan, M., Alarousu, E., Buin, A., et al. (2015). Low trap-state density and long carrier diffusion in organolead trihalide perovskite single crystals. *Science* 347, 519–522. doi: 10.1126/science.aaa2725
- Stranks, S. D., and Snaith, H. J. (2015). Metal-halide perovskites for photovoltaic and light-emitting devices. *Nat. Nanotechnol.* 10, 391–402. doi: 10.1038/nnano.2015.90
- Sun, H., Lei, T., Tian, W., Cao, F., Xiong, J., and Li, L. (2017). Self-powered, flexible, and solution-processable perovskite photodetector based on low-cost carbon cloth. *Small* 13:1701042. doi: 10.1002/sml.201701042
- Taylor, N. K., Abdi-Jalebi, M., Gupta, V., Hu, H., Dar, M. I., Li, G., et al. (2020). Recent progress in morphology optimization in perovskite solar cell. *J. Mater. Chem. A* 8, 21356–21386. doi: 10.1039/d0ta00143k
- Tan, Z. K., Moghaddam, R. S., Lai, M. L., Docampo, P., Higler, R., Deschler, F., et al. (2014). Bright light-emitting diodes based on organometal halide perovskite. *Nat. Nanotechnol.* 9, 687–692.
- Tang, F., Chen, Q., Chen, L., Ye, F., Cai, J., and Chen, L. (2016). Mixture interlayer for high performance organic-inorganic perovskite photodetectors. *Appl. Phys. Lett.* 109:123301. doi: 10.1063/1.4963269
- Tang, G., You, P., Tai, Q., Yang, A., Cao, J., Zheng, F., et al. (2019). Solution-phase epitaxial growth of perovskite films on 2D material flakes for high-performance solar cells. *Adv. Mater.* 31:e1807689.
- Tong, S., Sun, J., Wang, C., Huang, Y., Zhang, C., Shen, J., et al. (2017). High-performance broadband perovskite photodetectors based on CH3NH3PbI3/C8BTBT heterojunction. *Adv. Electron. Mater.* 3:1700058. doi: 10.1002/aelm.201700058
- Wang, J., Xiao, S., Qian, W., Zhang, K., Yu, J., Xu, X., et al. (2021). Self-driven perovskite narrowband photodetectors with tunable spectral responses. *Adv. Mater.* 33:e2005557.
- Wang, Q., Shao, Y., Dong, Q., Xiao, Z., Yuan, Y., and Huang, J. (2014). Large fill-factor bilayer iodine perovskite solar cells fabricated by a low-temperature solution-process. *Energy Environ. Sci.* 7, 2359–2365. doi: 10.1039/c4ee00233d
- Wang, W., Zhang, F., Bai, H., Li, L., Gao, M., Zhanga, M., et al. (2016). Photomultiplication photodetectors with P3HT: fullerene-free material as the active layers exhibiting a broad response. *Nanoscale* 8, 5578–5586. doi: 10.1039/c6nr00079g
- Wang, X., Huang, Y., Lei, W., Li, Q., Zhang, X., Khan, Q., et al. (2017). Asymmetrical photodetection response of methylammonium lead bromide perovskite single crystal. *Cryst. Res. Technol.* 52:1700115. doi: 10.1002/crat.201700115
- Wang, X., Li, Y., Xu, Y., Pan, Y., Zhu, C., Zhu, D., et al. (2020). Solution-processed halide perovskite single crystals with intrinsic compositional gradients for x-ray detection. *Chem. Mater.* 32, 4973–4983. doi: 10.1021/acs.chemmater.9b05000
- Wang, X., Wu, Y., Li, G., Li, Y., Wu, J., Zhang, X., et al. (2019a). Fabrication of photodiodes based on solution-processed perovskite single crystals. *IEEE Trans. Electron Devices* 66, 485–490. doi: 10.1109/ted.2018.2878828
- Wang, X., Wu, Y., Li, G., Wu, J., Zhang, X., Li, Q., et al. (2018). Ultrafast ionizing radiation detection by p-n junctions made with single crystals of solution-processed perovskite. *Adv. Electronic Mater.* 4:1800237. doi: 10.1002/aelm.201800237
- Wang, X. D., Li, W. G., Liao, J. F., and Kuang, D. B. (2019b). Recent advances in halide perovskite single-crystal films: fabrication methods and optoelectronic applications. *Solar RRL* 3:1800294. doi: 10.1002/solr.201800294
- Wang, Y., Shi, Y., Xin, G., Lian, J., and Shi, J. (2015). Two-dimensional van der Waals epitaxy kinetics in a three-dimensional perovskite halide. *Cryst. Growth Des.* 15, 4741–4749. doi: 10.1021/acs.cgd.5b00949
- Wang, Y., Yang, F., Li, X., Ru, F., Liu, P., Wang, L., et al. (2019c). Epitaxial growth of large-scale orthorhombic CsPbBr3 perovskite films with anisotropic photoresponse property. *Adv. Funct. Mater.* 29:1904913. doi: 10.1002/adfm.201904913
- Wei, H., Desantis, D., Wei, W., Deng, Y., Guo, D., Savenije, T. J., et al. (2017). Dopant compensation in alloyed CH3NH3PbBr3-xClx perovskite single crystals for gamma-ray spectroscopy. *Nat. Mater.* 16, 826–833. doi: 10.1038/nmat4927
- Wu, H., Chu, B., and Su, Z. (2020). Improved performance of perovskite photodetectors with a hybrid planar-mixed heterojunction. *Mater. Res. Exp.* 7:066201. doi: 10.1088/2053-1591/ab98c9
- Xing, G., Mathews, N., Lim, S. S., Yantara, N., Liu, X., Sabba, D., et al. (2014). Low-temperature solution-processed wavelength-tunable perovskites for lasing. *Nat. Mater.* 13, 476–480. doi: 10.1038/nmat3911
- Xu, Y., Wang, X., Pan, Y., Li, Y., Emeka Elemike, E., Li, Q., et al. (2020). Perovskite photodetectors based on p-i-n junction with epitaxial electron-blocking layers. *Front. Chem.* 8:811. doi: 10.3389/fchem.2020.00811
- Yakunin, S., Dirin, D. N., Shynkarenko, Y., Morad, V., Cherniukh, I., Nazarenko, O., et al. (2016). Detection of gamma photons using solution-grown single crystals of hybrid lead halide perovskites. *Nat. Photonics* 10, 585–589. doi: 10.1038/nphoton.2016.139
- Yang, D., Yang, Z., Qin, W., Zhang, Y., Liu, S., and Li, C. (2015). Alternating precursor layer deposition for highly stable perovskite films towards efficient solar cells using vacuum deposition. *J. Mater. Chem. A* 3, 9401–9405.
- Yang, M., Zeng, Y., Li, Z., Kim, D. H., Jiang, C. S., Van De Lagemaat, J., et al. (2017). Do grain boundaries dominate non-radiative recombination in CH3NH3PbI3 perovskite films? *Phys. Chem. Chem. Phys.* 19, 5043–5050.
- Zhang, F., Song, J., Zhang, L., Niu, F., Hao, Y., Zeng, P., et al. (2016). Film-through large perovskite grains formation via a combination of sequential thermal and solvent treatment. *J. Mater. Chem. A* 4, 8554–8561.
- Zhang, M., Zhang, F., Wang, Y., Zhu, L., Hu, Y., Lou, Z., et al. (2018). High-performance photodiode-type photodetectors based on polycrystalline formamidinium lead iodide perovskite films. *Sci. Rep.* 8:11157.

Conflict of Interest: The authors declare that the research was conducted in the absence of any commercial or financial relationships that could be construed as a potential conflict of interest.

Copyright © 2021 Xu, Wang, Zhao, Pan, Li, Elemike, Li, Zhang, Chen, Zhao, Akram, Bae, Bin and Lei. This is an open-access article distributed under the terms of the Creative Commons Attribution License (CC BY). The use, distribution or reproduction in other forums is permitted, provided the original author(s) and the copyright owner(s) are credited and that the original publication in this journal is cited, in accordance with accepted academic practice. No use, distribution or reproduction is permitted which does not comply with these terms.